Time-Dependent Density Functional Theory Description of On-Site Electron Repulsion and Ligand Field Effects in the Optical Spectrum of Hexaaquoruthenium(II) in Solution

Leonardo Bernasconi and Michiel Sprik*

Department of Chemistry, University of Cambridge, Lensfield Road, Cambridge CB2 1EW, U.K.

Received: January 20, 2005; In Final Form: April 19, 2005

Time-dependent density functional theory (TDDFT) and density functional-based molecular dynamics were used to simulate the finite temperature $t_{2g}^5e_g \leftarrow t_{2g}^6$ absorption band of the Ru^{2+} hexahydrate coordination complex in aqueous solution. The $^1T_1 \leftarrow {}^1A_1$ and $^1T_2 \leftarrow {}^1A_1$ molecular term splitting of this transition, which is not accounted for by the Kohn−Sham excitation spectrum, is shown to be satisfactorily reproduced by TDDFT at the BLYP/ALDA level of theory. Comparison to the spectrum of the $Ru^{2+}(H_2O)_6$ complex in vacuo computed by similar density functional classical molecular dynamics methods leads to the observation that bulk solvation has a negligible effect on the position and the shape of the absorption profile.

I. Introduction

The ultraviolet and visible absorption spectra of aqueous transition-metal cations are usually assigned and interpreted in terms of symmetry and strength of the crystal (or ligand) field originating from water molecules directly coordinated to the ion.[1] The effect of the solvent medium beyond the ligand molecules is more difficult to describe quantitatively through experimental methods, because most complexes are not easy to study in isolation. For computational methods, the stabilization of a cationic complex in vacuo is however easily achieved. Furthermore, the development of TDDFT[2,3] methods and their application to large-scale extended (periodic) systems has paved the way to a complete and possibly quantitative characterization of many spectroscopic properties of solvated systems, explicitly treating the solvent environment at the same level of theory as the optically active solute complex.

In a recent study of the optical properties of the two closed-shell (d^{10}) Ag^+ and Cu^+ metal ions in aqueous solution,[4] we analyzed in detail the performance of TDDFT in accounting for transitions involving transfer of electrons from the split manifold of (fully occupied) d orbitals to states arising from hybridization between an unoccupied metal-ion s Rydberg-like orbital and the bottom of the conduction band of the solvent. The explicit account of the detailed electronic structure of the bulk solvent, as well as of that of the solute ion, was therefore in this case a prerequisite for a satisfactory description of the spectroscopic properties of the solute. As revealed by recent theoretical work, transitions to Rydberg states[5] or excitations carrying large charge-transfer character[6−8] are highly problematic cases for generalized gradient approximation (GGA)-based implementations of TDDFT, as the one employed in our approach. In our calculations, this resulted in a rather inaccurate TDDFT estimate for the absolute value of the thermally averaged d → (s + water) transition energy, as compared to experiment. Most spectral features of Ag^+ and the overall spectral profile were, on the other hand, satisfactorily reproduced. Besides, these features could successfully be explained in terms of a simple model for the splitting of a localized (occupied) d manifold of states in an average dihedrally distorted tetrahedral coordination. Our results for the Ag^+ aqua ion can therefore be seen as a validation of the classic crystal-field (CF) picture for this ion in solution. (This conclusion could not however be carried over to the Cu^+ UV spectrum, which was found to be dominated by solvent thermal fluctuations.) Hybrid (Hartree−Fock exchange) DFT and TDDFT schemes[6] were shown to improve the numerical agreement with experiment, without nonetheless delivering accuracy comparable to gas-phase molecular calculations.

The work described in the present publication aims at assessing the applicability and accuracy of TDDFT to a d → d transition in a classic[9] open-shell transition metal aqua ion, the Ru^{2+} hexahydrate complex, in bulk solution at room temperature (for a related study of the redox chemistry of this system, see ref 10). In classical CF theory, transitions with nonnegligible probability are induced between split manifolds of d states which are well-localized on the ion center. In this respect, the d → d excitations bear resemblance to typical *valence* transitions in molecules, such as the $n \rightarrow \pi^*$ band of acetone, which we have previously investigated using similar methods.[11,12] TDDFT is expected in these cases to yield a fairly accurate account of low-energy excited-state properties of transition-metal compounds, even in the limit of simple approximations to both the exchange-correlation functional and the kernel. This claim is supported by several calculations described in the literature.[13−16]

There is however one important feature which sets the optical absorption of octahedral transition-metal coordination complexes apart from the spectrum of small molecules such as acetone. The cubic symmetry of the crystal field is sufficiently high to allow for orbital degeneracy in the localized d manifold, which can give rise to electronic term splittings of a magnitude comparable to atomic values. The Ru^{2+} hexahydrate with its singlet t_{2g}^6 ground-state configuration is one of the simplest examples of this effect, which is ultimately a manifestation of interelectron Coulomb repulsion in the excited state. This interaction is *not* included in the independent-particle Kohn−Sham model underpinning the TDDFT formalism, although it is described exactly in TDDFT by the Hartree contribution to the time-dependent kernel. Irrespective of the approximation adopted for the exchange-correlation kernel, this effect is therefore guaranteed to be accounted for properly by TDDFT.

A second concern is the effect of the solvent. The electron repulsion is usually quantified in terms of Racah parameters of

10.1021/jp0503718 CCC: $30.25
Published on Web 05/28/2005

which the parameter *B* is the most sensitive to the formation of coordination bonds.[9,17] The reduction of *B* in the complex as compared to the free-ion value is an experimental measure of the delocalization of the ionic charge over the ligands (*nephelauxetic effect*). This raises the issue of the extent to which *B* is affected by solvent *beyond* the first solvation shell. This important aspect of the chemistry of transition-metal aqua ions has also been addressed in the present study.

II. Relevant Elements of Ru(II) Coordination Chemistry

The aqueous chemistry of Ru^{2+} has been the subject of a substantial number of studies both experimental[18−20] and theoretical.[21] Interest in this system is motivated by promising applications to synthetic organometallic processes, owing to the tendency of the aqueous ion to coordinate large classes of ligands including N-heterocycles and olefins, as well as small gaseous molecules (H_2, N_2, C_2H_4, CO). Ru^{2+} aqua complexes have also been identified as key intermediates in metabolic cycles associated to the antitumor activity of Ru(II) compounds and as catalytic agents for isomerization and polymerization of olefins.[22]

Hydrated Ru(II) occurs as an octahedral (O_h) low-spin t_{2g}^6 complex, $Ru(OH_2)_6^{2+}$. Ligand-field splitting of the metal-ion 4d orbital manifold leads to a set of fully occupied t_{2g} states (d_{xy}, d_{xz}, d_{yz}) spread out between the ligands, and empty e_g ($d_{x^2-y^2}$, d_{z^2}) states pointing toward the ligands. The three t_{2g} orbitals have largely nonbonding character, while the empty e_g states are the antibonding partners of two σ coordination bonds of the same symmetry. In comparison to the free ion, the relative energies of the t_{2g} and e_g states are -4 *Dq* and 6 *Dq*, respectively. Coordination of water molecules beyond the first solvation shell is hindered by the orientation of the t_{2g} orbitals, which prevents a seventh molecule from approaching a face or an edge of the octahedron.

In an octahedral environment, with vibrational motion breaking the inversion symmetry, six $t_{2g}^5e_g \leftarrow t_{2g}^6$ transitions are possible, which are degenerate in the absence of interaction between t_{2g} and e_g electrons. Interelectron repulsion splits the corresponding transition energies into two groups. The $d_{z^2} \leftarrow d_{xy}$ transition promotes one electron off the *xy* plane along the *z*-axis direction, producing a particle−hole pair of T_2 symmetry. Since d_{xz} and d_{yz} orbitals are both occupied, this process results in additional charge accumulating along the *z* axis. By contrast, the $d_{z^2} \leftarrow d_{xz}$ and $d_{z^2} \leftarrow d_{yz}$ transitions simply relocate electron charge along the *z* axis. The charge distributions in the corresponding T_1 particle−hole pairs is still fairly similar to the ground state, whereas the T_2 excitation brings about an overall increase in electron repulsion, with an associated *positive* shift in transition energies as compared to the independent-electron picture. As a result of electron interaction, two peaks occur in the absorption spectrum, at energies other than $\Delta_o = 10\ Dq$. Their separation is related to Δ_o via the Racah parameter *B*.[9,17]

Visible spectra of Ru^{2+} in solution have been obtained in the presence of either tetrafluoroborate or *p*-toluenesulfonate anions, and they are found to be identical above ∼3.6 eV.[18] Two broad absorption bands at 2.34 and 3.18 eV with relative intensities at the maximum of absorption of ∼0.7 were attributed to ligand-field (LF) $^1T_1 \leftarrow {}^1A_1$ and $^1T_2 \leftarrow {}^1A_1$ transitions, respectively. From these assignments, with the method of Tanabe and Sugano,[23] values for *Dq* and *B* were obtained of 0.27 and 6.3×10^{-2} eV, respectively.

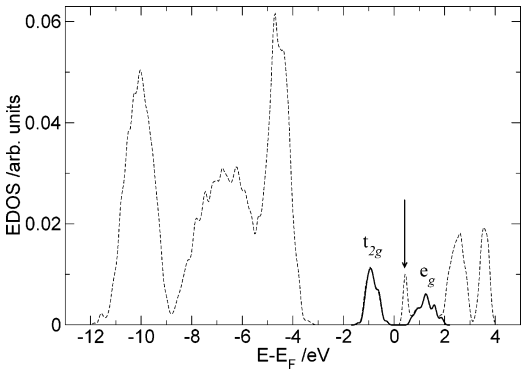

Figure 1. Room-temperature Kohn−Sham EDOS for Ru^{2+} in aqueous solution. The thick continuous line represents the contribution from orbitals with large metal-ion d character. Labeling is conventional (see also Figure 2). The arrow indicates the position of the lowest unoccupied orbital. Energies are relative to the Fermi energy E_F (highest occupied molecular orbital of the solution). A Gaussian convolution of standard deviation $\sigma = 0.05$ eV has been used in the plot.

III. Details of Calculations

DFT calculations and ab initio molecular dynamics (AIMD) simulations were performed using *CPMD*.[24] Norm-conserving fully separable[25] ab initio pseudopotentials of the Troullier−Martins type[26] were employed, with s and p nonlocal projectors for O (pseudization radius 1.05 au) and a local s potential for H. The pseudopotential parameters for Ru were taken from ref 22. The electron configuration [Kr] $4d^7$ of Ru^+ is taken as a reference state, and the 4s, 4p, and 4d electrons are treated as valence. The pseudization radii are 1.1 au for the s channel, 1.2 for p, and 1.24 for d. The Kleinman−Bylander transformation was used for O, and the Gauss−Hermite integration for Ru. All pseudopotentials were generated by inversion of the all-electron calculations performed at the BLYP[27,28] level of theory.

The solvated ion was treated within periodic boundary conditions using a cubic supercell of size $a = 9.86$ Å containing 1 metal atom and 32 water molecules. Charge neutrality was enforced through the introduction of a uniform neutralizing background, replacing a counterion of charge -2 at infinite dilution. Calculations on $Ru(OH_2)_6^{2+}$ in the gas phase were performed using cluster boundary conditions[29] with a supercell parameter $a = 15.00$ Å. One-particle wave functions were expanded in plane waves at the Γ point of the Brillouin zone up to a kinetic energy cutoff of 70 Ry. Constant-volume AIMD simulations were performed using the Car−Parrinello method[29−31] in BLYP approximation. A fictitious mass of 800 au and a time step of 5 au were used in the integration of the equations of motion. The simulation temperature was set to 300 K and controlled through a Nosé-Hoover thermostat. Total simulation times were 5 ps for the solution and 2 ps for the gas-phase cluster. Excitation energies and transition intensities were estimated within the Tamm−Dancoff approximation[32−34] from instantaneous atomic configurations extracted from the AIMD simulations. The TDDFT response equations were solved using Davidson's iterative subspace method.[35]

IV. Electronic and Optical Properties of The Solvated Ion

The Kohn−Sham electron density of states (EDOS) of aqueous Ru^{2+} obtained from 32 instantaneous ionic configurations (spanning an overall simulation time of 2 ps) is shown in Figure 1. Three occupied states next to the Fermi energy are largely concentrated on the metal-ion center (Figure 2) and are spread in energy over a range of ∼0.5 eV. These Kohn−Sham

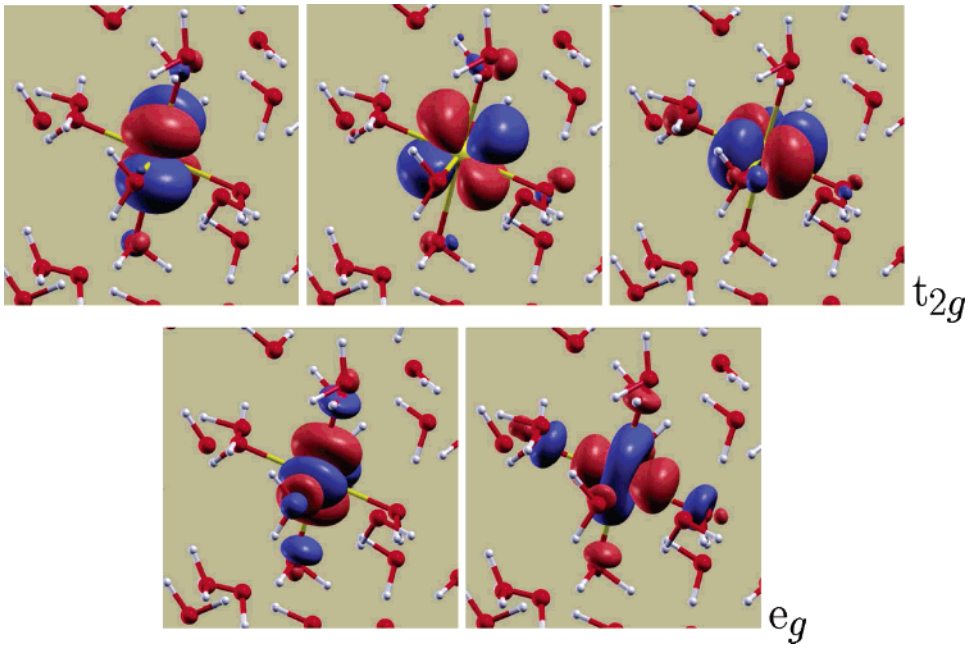

Figure 2. Aqueous Ru^{2+}: Selected occupied (upper panels) and unoccupied Kohn−Sham orbitals. Different colors are used to identify the phase of the wave function. Surfaces represent regions of constant electron density $\rho = \pm 0.075$ bohr^{-3}. The Ru^{2+} ion is located roughly at the center of each plot. The orbitals conventionally indicated here as t_{2g} correspond to the highest, second highest, and third highest occupied. The e_g orbitals are the *second* and *third* lowest unoccupied states.

states will *conventionally* be identified with the t_{2g} manifold of CF orbitals, because they closely resemble corresponding orbitals in the zero-temperature gas-phase complex. The onset of the conduction band of water is marked by the occurrence of a semilocalized state ∼4.5 eV above the solvent valence band edge (which corresponds to the peak at approximately −4 eV). This result is consistent with previous BLYP calculations on bulk clean water and various solvated ions, yielding an energy gap $E_g \simeq 4.5$ eV.[11] The second and third lowest empty states, responsible for a symmetric band in the EDOS from 0.5 to 2 eV, correspond to the e_g states of CF theory.

As discussed in ref 4, semilocalized empty orbitals detached from the bottom of the conduction band of pure water (whose existence has been proposed in an attempt to explain features in the low-energy absorption region of the liquid[36]) appear here at too low an energy. This has been attributed to deficiencies of the BLYP approximation in the density functional. Such states extend over several angstroms, and at the length scale of our simulation supercell, they may well be regarded as genuine conduction states. The positions of the energy levels of localized states, such as the metal d manifold, are however much more reliable. The ordering of the e_g and water last unoccupied molecular orbital (LUMO) shown Figure 1 is therefore likely to be incorrect. Arguably, the e_g state should correspond to the true LUMO of the solution. No orbital mixing between metal and water molecule states is observed beyond the first coordination shell, which points toward the absence of hybridization between metal-ion orbitals and extended states belonging to the conduction band of the solvent. These observations will turn out to be essential for gauging the accuracy of TDDFT spectra obtained using the density of states of Figure 1 as reference.

The Tamm−Dancoff TDDFT absorption spectrum (Figure 3) was computed from the same set of instantaneous ionic configurations, with only 14 lowest-energy excitations included in the calculation. Assignments of subsets of TDDFT transitions to one-particle Kohn−Sham excitations were obtained following the procedure detailed in ref 11. The lowest-energy region of the spectrum (0.5−2 eV) is dominated by a relatively weak tail

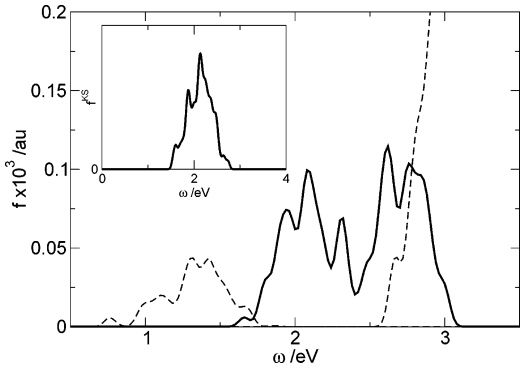

Figure 3. Resolved TDDFT absorption spectrum of solvated Ru^{2+} at room temperature. The thick line represents the contribution from the 6 $e_g \leftarrow t_{2g}$ transitions; the dashed lines mark spectral regions dominated by electronic excitations involving solvent states. Only the 14 excitations of lowest energy have been included. The inset shows the function f^{KS} of eq 1 proportional to the Kohn−Sham $e_g \leftarrow t_{2g}$ partial spectrum (see text for details), in arbitrary units. A Gaussian smearing of standard deviation $\sigma = 0.025$ eV has been introduced in all plots.

of transitions from the t_{2g} orbitals to the lowest unoccupied (solvent) state. Each of these 3 transitions results in 1 electron being excited from the metal center to the delocalized LUMO of the solvent. Transitions between t_{2g} and e_g orbitals on the metal center were found to give rise to two main bands, centered at $\omega_1 = 2.1$ and $\omega_2 = 2.6$ eV, of comparable intensity and a slightly less spread-out distribution for the higher-energy one. The spectral profile above ∼2.5 eV is dominated by strong solvent valence → conduction band transitions.

As thoroughly discussed in refs 4 and 11, electronic transitions between states well-localized on the same atomic center may be extremely well accounted for by TDDFT, even within adiabatic (frequency independent) and local approximations to the exchange-correlation kernel. This observation gives us confidence in the accuracy of the energies for the transitions identified by our assignment as d → d (indicated by solid lines in Figure 3). In contrast, the bands represented by dashed lines in the calculated spectrum must be a spurious effect, attributable

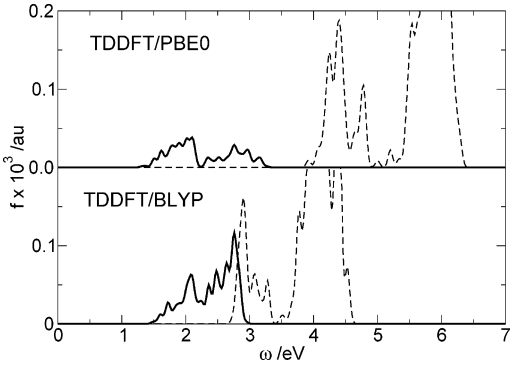

Figure 4. Resolved room-temperature BLYP and PBE0 TDDFT absorption spectra of gas-phase $Ru(OH_2)_6^{2+}$. Both spectra have been obtained from the same set of 21 instantaneous atomic configurations (spanning an overall time of 2.5 ps) extracted from an AIMD simulation which was carried out at the BLYP level of theory. Details of the plots are similar to Figure 3.

to severe underestimation of the one-particle energy gap in the pure liquid (shifting the water LUMO down to lower energies) and the approximations adopted in modeling the time-dependent response. Indeed, experimental spectra of Ru^{2+} solutions indicate vanishingly small absorption below ~1.5 eV.[18] This situation bears obvious resemblance with the charge-transfer problem in large molecules in the gas phase.[6,7] The inadequacy of TDDFT at describing charge-transfer excitations is largely explained by the absence of two-particle correlations in most currently available local (and adiabatic) exchange-correlation kernels,[8] which results in a poor description of the interaction between *localized* particles and holes at moderate distances ("bound excitons"). Further complications arise in the present case from the change in the localization properties of electrons upon excitation, a phenomenon which is rather related to the dielectric response of the medium following the particle−hole pair creation.[37]

We have shown[12] that suitable extensions of the TDDFT response equations to include "exact" (Hartree−Fock) exchange (both in the calculation of the reference ground state *and* in the solution of the corresponding time-dependent coupled-perturbed Kohn−Sham equations) inhibit charge transfer like excitations at unphysically low energies in solvated systems (solution or small gas-phase clusters). These approaches do *not* require explicitly modifying the form of the exchange-correlation kernel (e.g., wrt ALDA[38]) and are therefore straightforwardly implemented in conventional TDDFT codes (unfortunately greatly adding to the computational costs when used in combination with plane wave basis sets). Furthermore, we have established that, as long as the electronic coupling (orbital mixing) between solute and solvent states remains negligible, transitions between localized states are accounted for to essentially the same accuracy by local and (in the sense just indicated) hybrid schemes.[11,12]

We verified that a similar separation between localized d → d and (partially) delocalized transitions involving solvent states can be achieved in the present situation, using gas-phase $Ru(OH_2)_6^{2+}$ as a model for the solvated ion. The room-temperature absorption spectra obtained using TDDFT/BLYP and TDDFT/PBE0[12] are shown in Figure 4. In both cases, metal-ion transitions are responsible for a broad absorption region at $\omega = 1.5-3$ eV, which in the TDDFT/PBE0 case is separated by a gap of ~1 eV from the lowest excitation involving water molecule orbitals (mainly σ^* states). The ligand field (LF) absorption range is left virtually unchanged in both spectra, which lends support to the accuracy of the results obtained on the solvated ion at the BLYP level of theory. Furthermore, when comparing Figures 3 and 4, no solvent shift is observed in the LF transitions in going from the gas-phase cluster to the solvated ion. This is consistent with the fact that $t_{2g}^5e_g \leftarrow t_{2g}^6$ transitions do not induce low-order multipole moments in the electron density distribution of the metal ion, and they are therefore negligibly affected by electrostatic interactions with the bulk solvent.

The average position of the absorption band (approximately coinciding with the minimum at 2.4 eV in Figure 3) is red-shifted by 0.35 eV relative to the corresponding feature in the experimental spectrum.[18] The ratio between the frequency at the maximum of absorption of the two $e_g \leftarrow t_{2g}$ bands is $\omega_2/\omega_1 = 1.29$ (experimental 1.34). Using the same graphical approach of Tanabe and Sugano[9,17,23] as applied to the experimental data, we can extract from the computed spectrum an estimate for the crystal field Δ_o and Racah parameter B. We obtain $\Delta_o = 2.23$ eV which should be compared to the experimental value of $\Delta_o = 2.73$ eV and $B = 0.052$ eV (experimental $B = 0.063$ eV). Both energies are therefore 15−20% too low. Considering the approximations implicit in the approach adopted, we regard this result to be in fair agreement with experiment. Note that the reference Kohn−Sham energy levels (Figure 1) yield a very similar estimate of the octahedral splitting $\Delta_o = 2.1$ eV. The Kohn−Sham spectral profile does however lack the double-peak structure of the TDDFT spectrum, and the spread in energy of the Kohn−Sham transition energies is exclusively of thermal origin. This can be seen most clearly by plotting the function

$$f^{KS}(\omega) = \sum_{t_{2g}}\sum_{e_g} \delta(\omega - \epsilon_{e_g}^{KS} + \epsilon_{t_{2g}}^{KS}) \qquad (1)$$

where $\epsilon_{e_g,t_{2g}}^{KS}$ are Kohn−Sham orbital energies, representing the $t_{2g}^5e_g \leftarrow t_{2g}^6$ Kohn−Sham absorption under the approximation that all transitions contribute with the same finite probability to the profile (see inset of Figure 3). The distinction between $^1T_1 \leftarrow {}^1A_1$ and $^1T_2 \leftarrow {}^1A_1$ excitations originates from many-body relaxation following the Kohn−Sham particle−hole pair creation, and it therefore manifests itself as a purely time-dependent phenomenon starting from the one-particle Kohn−Sham model. At this point, it is perhaps useful to reiterate that the excitation energies in our approach correspond to strictly vertical excitations. The finite intensity of octahedral complexes in dipole forbidden transitions is therefore entirely the result of thermal fluctuations reducing the symmetry. Vibronic coupling is neglected in our approach (for TDDFT-based vibronic calculation, see for example ref 16).

Our estimate of the Racah parameter B is in reasonable agreement with experiment, confirming that the Coulomb repulsion between electrons localized on the metal-ion center is accounted for properly, if possibly only semiquantitatively, by TDDFT, even within BLYP/ALDA. This is a direct consequence of the fact that the response of the Coulomb potential to a perturbation is treated *exactly* in TDDFT via the Hartree kernel $f_H = 1/|\mathbf{r} - \mathbf{r}'|$, which does not depend on the approximation used for the static exchange-correlation potentials and for the exchange-correlation kernel. The physical mechanism responsible for the occurrence of two molecular terms $^1T_1 \leftarrow {}^1A_1$ and $^1T_2 \leftarrow {}^1A_1$ from a single excited configuration $t_{2g}^5e_g \leftarrow t_{2g}^6$ does not involve direct screened particle−hole interaction, and it is therefore properly described by local exchange-correlation functionals and kernels. This result is particularly relevant for future applications of TDDFT to transition metals in the condensed phase and in large molecular systems.

V. Conclusions

The room-temperature absorption spectrum of Ru^{2+} in solution has been computed from TDDFT and AIMD at the BLYP level of theory. The contribution of LF transitions to the overall spectral profile has been isolated via resolution into elementary Kohn−Sham excitation and by comparison to a similar calculation carried out on gas-phase $Ru(OH_2)_6^{2+}$ at a higher level of theory (PBE0). The BLYP exchange-correlation functional, in conjunction with an ALDA TDDFT kernel, was found to be sufficiently accurate to reproduce the experimental absorption spectrum to satisfactory accuracy. The occurrence of two absorption maxima was shown to arise from direct Coulomb interaction between excited e_g and t_{2g} electrons, supporting the experimental assignment to $^1T_1 \leftarrow {}^1A_1$ and $^1T_2 \leftarrow {}^1A_1$ transitions. Values for the octahedral field splitting Δ_o and the Racah parameter B were computed in reasonable agreement with experiment. Furthermore, our calculations suggest that these parameters are almost completely determined by the interaction of orbitals localized on the Ru center with states belonging exclusively to the six ligand water molecules and are virtually insensitive to the presence of the bulk solvent.

Acknowledgment. This work is part of the 2001−2004 CCP1 flagship project supported by EPSRC. Computer resources were provided by the CLRC at Daresbury Laboratories and the UKCP, which gave us access to the HPCx facility at Daresbury.

References and Notes

(1) Deeth, R. J. *Faraday Discuss.* **2003**, *124*, 379.
(2) Runge, E.; Gross, E. K. U. *Phys. Rev. Lett.* **1984**, *52*, 997.
(3) Petersilka, M.; Gossmann, U. J.; Gross, E. K. U. *Phys. Rev. Lett.* **1996**, *76*, 1212.
(4) Bernasconi, L.; Blumberger, J.; Sprik, M.; Vuilleumier, R. *J. Chem. Phys*. **2004**, *121*, 11885.
(5) Tozer, D. J.; Amos, R. D.; Handy, N. C.; Roos, B. O.; Serrano-Andres, L. *Mol. Phys.* **1999**, *97*, 859.
(6) Dreuw, A.; Weisman, J. L.; Head-Gordon, M. *J. Chem. Phys.* **2003**, *119*, 2943.
(7) Dreuw, A.; Head-Gordon, M. *J. Am. Chem. Soc.* **2004**, *126*, 4007.
(8) Gritsenko, O.; Baerends, E. J. *J. Chem. Phys.* **2004**, *121*, 655.
(9) Shriver, D. F.; Atkins, P. W. *Inorganic Chemistry*, 3rd ed.; Oxford University Press: Oxford, 1999.
(10) Blumberger, J.; Sprik, M. *J. Phys. Chem. B* **2005**, *109*, 6793.
(11) Bernasconi, L.; Sprik, M.; Hutter, J. *J. Chem. Phys.* **2003**, *119*, 12417.
(12) Bernasconi, L.; Sprik, M.; Hutter, J. *Chem. Phys. Lett*. **2004**, *394*, 141.
(13) van Gisbergen, S. J. A.; Groenveld, J. A.; Rosa, A.; Snijders, J. G.; Baerends, E. J. *J. Phys. Chem. A* **1999**, *103*, 6835.
(14) Adamo, C.; Barone, V. *Theor. Chem. Acc.* **2000**, *105*, 169.
(15) Boulet, P.; Chermette, H.; Daul, C.; Gilardoni, F.; Rogemond, F.; Weber, J.; Zuber, G. *J. Phys. Chem. A* **2001**, *105*, 885.
(16) Neugebauer, J.; Baerends, E. J.; Nooijen, M. *J. Phys. Chem. B* **2005**, *109*, 116.
(17) Bersuker, I. B., Ed. *Electronic structure and properties of transition metal compounds*; Wiley & Sons: New York, 1996.
(18) Mercer, E. E.; Buckley, R. R. *Inorg. Chem.* **1965**, *4*, 1692.
(19) Bernhard, P.; Ludi, A. *Inorg. Chem.* **1984**, *23*, 870.
(20) Vito, D. D.; Sidorenkova, H.; Rotzinger, F. P.; Weber, J.; Merbach, A. E. *Inorg. Chem.* **2000**, *39*, 5547.
(21) Grundler, P. V.; Laurenczy, G.; Merbach, A. E. *Helv. Chim. Acta* **2001**, *84*, 2854.
(22) Handgraaf, J.-W.; Reek, J. N. H.; Meijer, E. J. *Organometallics* **2003**, 22, 3150.
(23) Tanabe, Y.; Sugano, S. *J. Phys. Soc. Jpn.* **1954**, *9*, 753.
(24) *CPMD*, version 3.8.2; IBM Zurich and MPI Stuttgart; see also www.cpmd.org.
(25) Kleinman, L.; Bylander, D. M. *Phys. Rev. Lett.* **1982**, *48*, 1425.
(26) Troullier, N.; Martins, J. L. *Phys. Rev. B* **1991**, *43*, 1993.
(27) Becke, A. *Phys. Rev. A* **1988**, *38*, 3098.
(28) Lee, C.; Yang, W.; Parr, R. G. *Phys. Rev. B* **1988**, *37*, 785.
(29) Marx, D.; Hutter, J. In *Modern Methods and Algorithms of Quantum Chemistry*; Grotendorst, J., Ed.; John von Neumann Institute for Computing: Jülich, 2000; Vol. 1, p 329.
(30) Car, R.; Parrinello, M. *Phys. Rev. Lett.* **1985**, *55*, 2471.
(31) Remler, D. K.; Madden, P. A. *Mol. Phys.* **1990**, *70*, 921.
(32) Hutter, J. *J. Chem. Phys.* **2003**, *118*, 3928.
(33) Fetter, A. L.; Walecka, J. D. *Quantum Theory of Many-Particle Systems*; McGraw-Hill: New York, 1971.
(34) Hirata, S.; Head-Gordon, M. *Chem. Phys. Lett.* **1999**, *314*, 291.
(35) Davidson, E. R. *J. Comput. Phys.* **1975**, *17*, 87.
(36) Bernas, A.; Ferradini, C.; Gerin, J.-P. *J. Photochem. Photobiol., A* **1998**, *117*, 171.
(37) Onida, G.; Reining, L.; Rubio, A. *Rev. Mod. Phys*. **2002**, *74*, 601.
(38) Casida, M. E. In *Recent Developments and Applications of Modern Density Functional Theory*; Seminario, J. M., Ed.; Elsevier: Amsterdam, 1996; Vol. 4, p 155.